CORROSION SCIENCE AND TECHNOLOGY, Vol.25, No.3(2026), pp.159~175 pISSN 1598-6462 / eISSN 2288-6524
[Research Paper] DOI: https://doi.org/10.14773/cst.2026.25.3.159

Time-Dependent Electrochemical Corrosion Characteristics of Coated Hot Press Forming Steels in Chloride Environment

Yu-Jin Choi, Ho-jun Choi, Yoori Kim, Ei-Joon Shim, and Hye-Jin Kim†

Department of Advanced Materials Engineering, Tech University of Korea (TU Korea), Siheung-si, Gyeonggi-do, 15073, Republic of Korea

(Received June 16, 2026; Revised June 24, 2026; Accepted June 24, 2026)

Hot-press-forming (HPF) steels require protective coatings to prevent oxidation and decarburization during high-temperature processing. This study investigated the corrosion behavior of Al–Si and galvannealed coated HPF steels in a 3.5 wt% NaCl solution, with immersion times of 1, 5, and 7 days. For the Al–Si coating, specimens were evaluated both with and without functional oil treatment. Open-circuit potential (OCP), electrochemical impedance spectroscopy (EIS), potentiodynamic polarization, and scanning electron microscopy (SEM) were employed to assess corrosion performance and degradation mechanisms. The Al–Si coated steels exhibited more noble corrosion potentials, lower corrosion current densities, and higher impedance values compared to the Zn-coated steel, indicating superior barrier-type corrosion protection. Functional oil treatment further improved the corrosion resistance of Al–Si coatings by promoting the formation of a thicker, more homogeneous oxide layer, which resulted in enhanced charge-transfer resistance throughout the immersion period. In contrast, the Zn-coated steel showed more negative corrosion potentials and lower impedance values due to sacrificial Zn dissolution. Surface observations revealed localized pitting corrosion in Al–Si coatings, associated with the breakdown of the oxide/intermetallic layer, whereas the Zn coating exhibited extensive formation of Zn-based corrosion products.

Keywords: *Hot-press forming, Al–Si coated HPF, Zn coated HPF, Functional oil, Electrochemical analysis*

1. Introduction

The drive toward lighter, safer passenger vehicles have made ultra-high-strength steels central to modern automotive body design, where reducing sheet thickness without compromising crash performance is a primary engineering goal [1,2]. Hot-press forming (HPF), also known as press hardening or hot stamping, has become the established route for producing such components: a boron-alloyed steel blank—most commonly 22MnB5—is austenitized at temperatures above approximately 900 °C, formed in a cooled die, and simultaneously quenched to a fully martensitic microstructure with tensile strengths exceeding 1500 MPa [3,4]. Hot-stamped parts are now standard in body-in-white structures such as A- and B-pillars, sills, and bumper beams, where their intrusion resistance contributes directly to occupant safety [5,6].

†Corresponding author: khj020911@tukorea.ac.kr
Yu-Jin Choi: Undergraduate student, Ho-jun Choi: Master's Student, Yoori Kim: Master's Student, Ei-Joon Shim: Master's Student, Hye-Jin Kim: Professor

A central difficulty of the HPF process is that austenitization in an oxidizing atmosphere causes severe surface oxide-scale formation and decarburization, which the lower surface hardness, impedes die-to-blank heat transfer, accelerates tool wear, and requires costly post-process shot blasting [7,8]. To suppress these effects, HPF blanks are almost always supplied with a protective metallic coating applied prior to heating [8,9]. Two coating systems dominate industrial practice and protect the substrate by fundamentally different mechanisms. Aluminum–silicon (Al–Si) coatings, applied by hot-dip aluminizing, transform during austenitization into a sequence of Fe–Al and Fe–Al–Si intermetallic layers that form a stable, adherent aluminum-oxide barrier; this layer limits oxygen ingress during forming and provides barrier-type corrosion protection in service [9,10,11]. Galvannealed coatings, by contrast, contain a Zn–Fe alloy (~10 wt% Fe) that protects the underlying steel sacrificially: zinc, being electrochemically more active than iron, preferentially dissolves and cathodically protects exposed substrate even where the coating is locally breached [12,13].

Because these two mechanisms respond very differently to chloride-bearing environments, their relative performance in service is not self-evident. Barrier-type Al–Si coatings rely on the integrity of the oxide/intermetallic layer, so localized defects can become sites of preferential attack, whereas sacrificial Zn coatings provide active protection but are progressively consumed as the zinc reservoir is depleted [13,14]. In quiescent NaCl solution, zinc-based coatings typically exhibit a markedly more negative corrosion potential consistent with sacrificial dissolution, while their long-term protectiveness declines as zinc is converted to corrosion products [14,15]. Chloride-induced corrosion is of practical relevance to automotive bodywork, where the perforation corrosion driven by deicing salt is a common failure mode [15]. A direct, time-resolved comparison of Al–Si and Zn coated HPF steels under identical chloride exposure is therefore needed to guide coating selection.

In addition, surface treatments applied during steel finishing can further influence corrosion behavior. Functional oils applied at the cold-rolling post-treatment line are used industrially to provide temporary protection and improve downstream processing, and such oil film may contribute an additional barrier to electrolyte penetration. The extent to which functional oil modifies the corrosion resistance of Al–Si coated HPF steel, however, has received limited systematic study.

In this work, the electrochemical corrosion behavior of Al–Si and Zn coated HPF steels was compared in 3.5 wt% NaCl solution as a function of immersion time (1, 5, and 7 days). For the Al–Si system, specimens prepared with and without a functional oil surface treatment were additionally examined to isolate the contribution of the oil layer. Open-circuit potential, electrochemical impedance spectroscopy, and potentiodynamic polarization measurements were combined with equivalent-circuit analysis and electron-microscopy observation of corrosion products to clarify the differing protection mechanisms and to evaluate the role of functional oil in enhancing barrier performance.

2. Experiment

2.1 Materials

Two coated hot-press-forming steel systems were

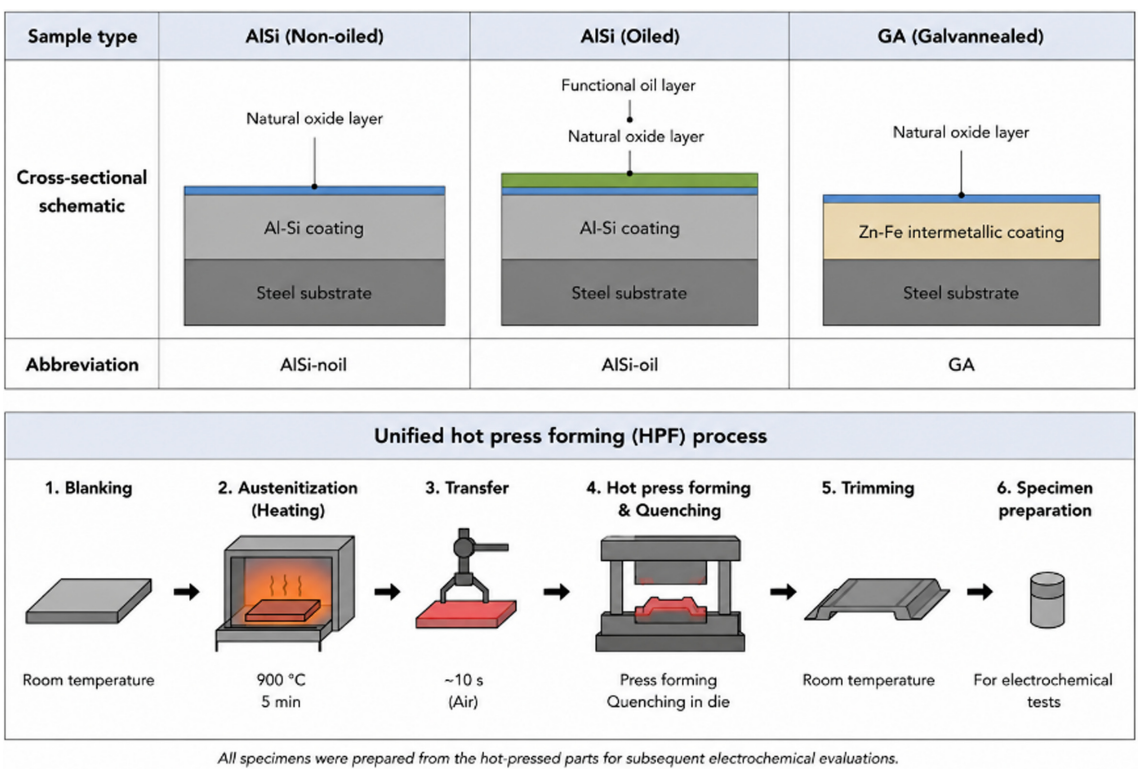

Fig. 1. Schematic illustration of the hot press forming (HPF) process and the resulting surface/interfacial layer structures of Al–Si and galvannealed coated steels under oiled and non-oiled conditions after austenitization, forming, and die quenching

investigated: Al–Si coated steel and a Zn coated steel. The Al–Si coated steel was supplied in two surface conditions — a non-oiled "Base" condition and an oiled "Functional" condition produced by applying a functional oil at the cold-rolling post-treatment line in Al-Si coating. The functional oil was applied at a coating weight of 0.1–10 g/m^2. The Zn coated steel was used in the received galvannealed condition.

Fig. 1 schematically summarizes the differences in coating evolution and expected corrosion behavior between Al–Si and Zn coated hot stamping steels after HPF processing. The Al–Si coating primarily acts as a barrier-type protective system through the formation of dense Al-rich oxide layers and Fe–Al intermetallic compounds during austenitization. In particular, the oiled Al–Si specimen is expected to exhibit improved corrosion resistance due to the formation of a thicker and more compact Al-oxide layer after thermal exposure. Such oxide thickening can suppress electrolyte penetration and retard charge transfer reactions at the coating/electrolyte interface.

In contrast, the Zn coated steel exhibits a fundamentally different corrosion mechanism governed by sacrificial Zn dissolution. During HPF, partial Zn evaporation and the formation of heterogeneous Fe–Zn intermetallic phases can generate discontinuous oxide regions and microstructural heterogeneity. These features may act as preferential pathways for localized corrosion initiation in chloride-containing environments. Although the Zn coating can initially provide cathodic protection to the steel substrate through active Zn dissolution, progressive Zn consumption during immersion is expected to reduce the long-term protective capability of the coating.

Therefore, the schematic in Fig. 1 conceptually illustrates the transition from barrier-dominated corrosion protection in Al–Si coatings to sacrificial corrosion protection in Zn coatings, highlighting the critical influence of functional oil treatment and post-HPF surface evolution on electrochemical corrosion behavior.

2.2 Specimen preparation

Specimens were cut to [2 cm × 2 cm] and an exposed area of 1 cm² was defined for electrochemical testing; the remaining surfaces were masked with mounting jig. Prior to immersion, specimens were degreased with ethanol and dried under N_2 — confirm cleaning procedure. Oiled specimens were tested with the functional oil layer intact and were not subjected to solvent decreasing, to preserve the as-applied surface condition.

2.3 Electrolyte and test conditions

All electrochemical measurements were carried out in 3.5 wt% NaCl solution prepared from reagent-grade NaCl and deionized water, at room temperature. Prior to testing, the electrolyte was deaerated by nitrogen purging to eliminate dissolved oxygen and ensure that the measured electrochemical response primarily reflected the corrosion behavior of the coated specimens. Measurements were performed after 1, 5, and 7 days of immersion to track the time evolution of corrosion behavior.

2.4 Electrochemical measurements

A conventional three-electrode cell was used, with the coated steel specimen as the working electrode, a saturated calomel / Hg/Hg_2Cl_2 reference electrode, and a platinum counter electrode, connected to a Gamry 1010B model. The open-circuit potential (OCP) was recorded for at least 30 min until a stable potential was reached. Electrochemical impedance spectroscopy (EIS) was then performed at the OCP using a sinusoidal perturbation of 10 mV (rms) over a frequency range of 100 kHz to 10 mHz. Finally, potentiodynamic polarization curves were measured from −0.5 V_{SCE} to +1.5 V_{SCE} versus the open-circuit potential at a scan rate of 5 mV s^{-1}. The corrosion potential (E_{corr}) and corrosion current density (i_{corr}) were determined by Tafel extrapolation of the anodic and cathodic branches.

2.5 Equivalent-circuit analysis

EIS spectra were fitted using equivalent electrical circuit models to quantify the protective performance of each coating. All materials were modeled with a single time constant, comprising the solution resistance (R_s), a constant-phase element representing the coating/double-layer capacitance (CPE_1), and the coating/charge-transfer resistance (R_1). Constant-phase elements were used in place of ideal capacitors to account for surface heterogeneity and frequency dispersion. Fitting quality is reported as the percentage error on each parameter.

2.6 Surface and microstructural analysis

The macroscopic appearance of the specimens was

recorded photographically after 7 days of immersion. The morphology and distribution of corrosion products were examined by scanning electron microscopy (SEM) after immersion, and corrosion phases were identified.

3. Results and Discussion

3.1 Microstructure observations

Fig. 2 shows the cross-sectional microstructures of the Al–Si and Zn coated steels after the hot press forming process. In the Al–Si coated specimen (Fig. 2a), distinct Fe–Al intermetallic layers composed mainly of Al_5Fe_2 and AlFe phases were observed above the martensitic substrate. These intermetallic compounds were formed through intensive Fe/Al interdiffusion during austenitization at elevated temperature. The multilayered intermetallic structure is characteristic of Al–Si coated hot stamping steels and is generally associated with improved oxidation resistance due to the formation of thermodynamically stable Al-rich oxide layers. However, the brittle nature of Fe–Al intermetallic compounds may also promote microcrack formation during forming and quenching, thereby providing preferential pathways for electrolyte penetration during corrosion exposure.

In contrast, the Zn coated steel (Fig. 2b) exhibited a Zn-containing α-Fe layer after HPF processing. The original Zn-rich coating was substantially transformed during austenitization because of Zn evaporation and Fe–Zn interdiffusion at high temperature. As a result, the coating became relatively heterogeneous compared with the Al–Si coated specimen. Such microstructural heterogeneity can contribute to localized galvanic activity and unstable corrosion behavior in chloride-containing environments. Nevertheless, the residual Zn-containing phases are still expected to provide sacrificial anodic protection during the initial stage of immersion.

These results indicate that the corrosion protection mechanisms of the two coatings are fundamentally different: the Al–Si coating primarily relies on barrier-type protection through dense intermetallic/oxide layers, whereas the Zn coating exhibits sacrificial protection governed by preferential Zn dissolution and localized electrochemical activity.

Fig. 3 compares the surface morphologies of Al–Si coated HPF steels after the hot press forming process under non-oiled and oiled conditions. Both specimens exhibited characteristic surface features associated with the formation of Fe–Al intermetallic compounds and thermally grown oxide layers during high-temperature austenitization. However, noticeable differences in surface morphology were observed depending on the application of functional oil prior to processing. The non-oiled Al–Si specimen (Fig. 3a) exhibited a relatively coarse and heterogeneous surface morphology with locally irregular features. Such non-uniform surface evolution suggests localized oxidation and uneven interdiffusion behavior during thermal exposure. The heterogeneous surface structure may facilitate localized electrolyte penetration and promote preferential corrosion initiation sites under chloride-containing environments.

In contrast, the oiled Al–Si specimen (Fig. 3b) showed a finer and more uniformly distributed network-like surface morphology. The functional oil is considered to influence oxidation kinetics during HPF, promoting the formation of a denser and more homogeneous oxide/intermetallic surface layer. This refined surface morphology can effectively reduce localized electrochemical heterogeneity and improve the barrier characteristics of the coating layer.

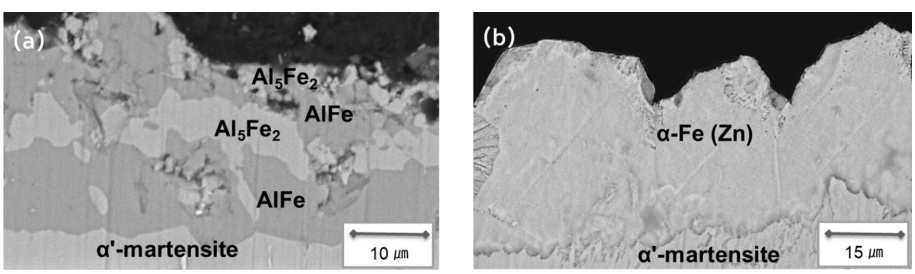

Fig. 2. Cross-sectional SEM images of the coating layers after hot press forming: (a) Al–Si coated HPF steel showing Fe–Al intermetallic compounds (Al_5Fe_2 and AlFe) formed on the martensitic substrate, and (b) Zn coated HPF steel exhibiting Zn-containing α-Fe layer formed after high-temperature processing

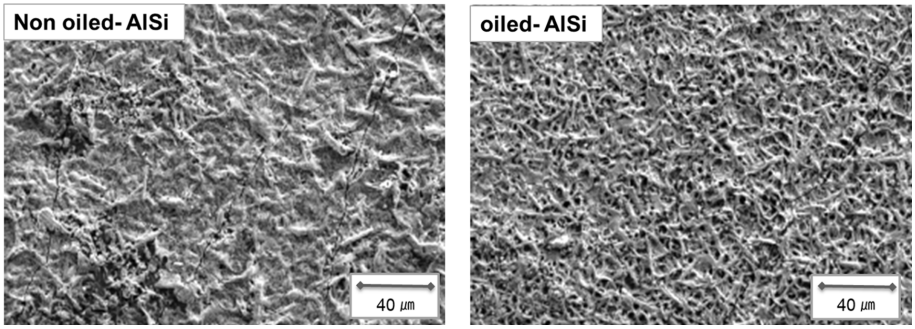

Fig. 3. Surface SEM images of Al–Si coated steels after hot press forming under (a) non-oiled and (b) oiled conditions

From a corrosion perspective, a more homogeneous surface structure is beneficial because it suppresses local galvanic coupling and limits the formation of preferential corrosion pathways. Therefore, the improved surface uniformity observed in the oiled Al–Si specimen is expected to contribute to the enhanced electrochemical stability and higher corrosion resistance observed during subsequent immersion testing.

3.2 Electrochemical test results

Fig. 4 shows the evolution of the open circuit potential (OCP) of the Al–Si and Zn coated HPF steels during immersion in 3.5 wt% NaCl solution. The OCP provides important insight into the thermodynamic stability and corrosion tendency of coating systems under chloride-containing environments.

The Al–Si coated steels exhibited relatively noble potentials compared with the Zn coated steel throughout the immersion period, indicating superior electrochemical stability. The non-oiled Al–Si specimen (Fig. 4a) also showed relatively noble potentials; however, a gradual decrease in OCP was observed during immersion. This behavior suggests progressive degradation of the protective surface layer due to chloride ion penetration through defects or microcracks within the Fe–Al intermetallic and oxide layers. The more unstable potential response compared with the oiled condition indicates reduced surface homogeneity and lower resistance to localized electrochemical activity. In particular, the oiled Al–Si specimen (Fig. 4b) maintained the most noble OCP values among all conditions, suggesting that the functional oil treatment enhanced the stability of the surface oxide/intermetallic layer formed during hot press forming. The gradual stabilization of the OCP with immersion time indicates the persistence of barrier-type corrosion protection, where the dense Al-rich oxide layer suppresses active electrochemical dissolution at the coating/electrolyte interface.

In contrast, the GA coated steel (Fig. 4c) exhibited significantly more negative OCP values throughout immersion, which is characteristic of sacrificial Zn-based coatings. The highly active potential originates from preferential anodic dissolution of Zn-containing phases, which cathodically protect the steel substrate. However, the continuous shift and instability in OCP with immersion time imply progressive Zn consumption and the

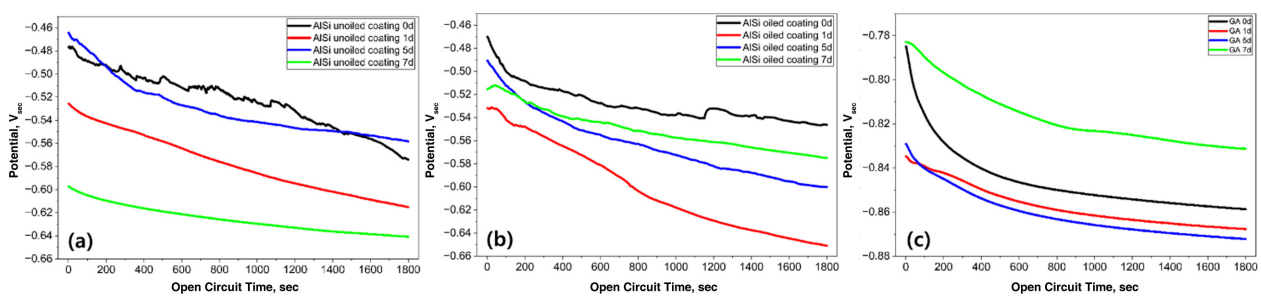

Fig. 4. Open circuit potential curves of (a) non-oiled Al–Si coated steel, (b) oiled Al–Si coated steel, and (c) Zn steel during immersion in 3.5 wt% NaCl solution

development of localized electrochemical heterogeneity during exposure to the chloride environment.

From a corrosion mechanism perspective, the OCP results clearly distinguish the dominant protection mechanisms of the two coating systems. The Al–Si coatings primarily exhibit passive/barrier-type protection governed by stable oxide formation, whereas the Zn coating relies on active sacrificial dissolution behavior. Furthermore, the improved potential stability of the oiled Al–Si specimen demonstrates that functional oil treatment contributes to the formation of a more electrochemically stable surface layer after HPF processing.

Fig. 5 presents the Nyquist plots of the Al–Si and Zn coated steels as a function of immersion time in 3.5 wt% NaCl solution. The electrochemical impedance response varied significantly depending on coating type and oil treatment condition, reflecting differences in corrosion protection mechanism and interfacial degradation behavior. Both Al–Si coated steels exhibited significantly larger capacitive semicircles than the Zn coated steel, indicating superior corrosion resistance associated with higher charge transfer resistance (R_{ct}).

For the non-oiled Al–Si specimen (Fig. 5a), the semicircle diameter initially increased during immersion and remained relatively large compared with the Zn coating. This behavior indicates that the Al-rich oxide layer still provided substantial barrier protection despite the absence of functional oil treatment. However, the distorted semicircle shape and gradual change in impedance response imply increasing interfacial heterogeneity and localized degradation caused by chloride penetration through defects and microcracks within the Fe–Al intermetallic layer. In particular, the oiled Al–Si specimen (Fig. 5b) showed the largest semicircle diameter among all conditions throughout the immersion period. This result suggests that the functional oil treatment promoted the formation of a denser and more protective oxide/intermetallic surface layer during hot press forming, thereby effectively suppressing electrolyte penetration and interfacial electrochemical reactions. The oiled Al–Si specimen exhibited a more stable capacitive response with a broader semicircle over the immersion period, suggesting improved electrochemical homogeneity and slower degradation kinetics. The relatively high impedance maintained even after prolonged immersion indicates that the dense oxide layer generated under the oiled condition effectively delayed charge transfer reactions and corrosion propagation at the coating/electrolyte interface. The slightly higher impedance observed after 7 days compared with 5 days is attributed to the partial accumulation of corrosion products on the surface, which temporarily hindered electrolyte transport and charge transfer reactions. Similar behavior has been reported in coated steels where corrosion products provide a transient barrier effect despite ongoing degradation.

In contrast, the Zn coated steel (Fig. 5c) showed substantially smaller semicircle diameters and a rapid reduction in impedance with immersion time. Such behavior is characteristic of active Zn dissolution and sacrificial corrosion protection mechanisms. Initially, the Zn-rich coating preferentially dissolves to cathodically protect the steel substrate; however, progressive Zn consumption leads to a decrease in coating resistance and promotes localized electrochemical heterogeneity. The depressed semicircle and reduced impedance response further indicate unstable corrosion product formation and accelerated interfacial degradation in the chloride-containing environment.

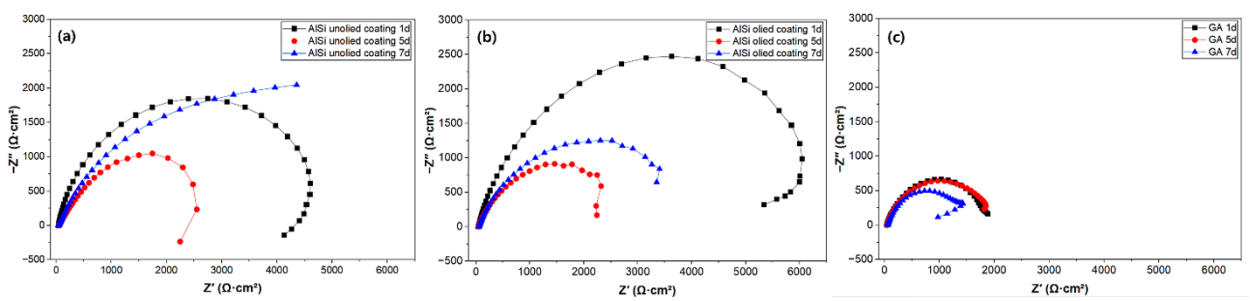

Fig. 5. Nyquist plots of (a) non-oiled Al–Si coated steel, (b) oiled Al–Si coated steel, and (c) Zn coated steel measured after immersion in 3.5 wt% NaCl solution for 1, 5, and 7 days

From an electrochemical standpoint, the Nyquist results clearly demonstrate that the Al–Si coatings primarily provide barrier-type corrosion protection through stable oxide/intermetallic layers, whereas the Zn coating relies on sacrificial anodic dissolution of Zn. Furthermore, the enlarged capacitive semicircle observed in the oiled Al–Si specimen confirms that functional oil treatment significantly enhances charge transfer resistance and improves long-term electrochemical stability after hot press forming.

Fig. 6 presents the Bode impedance and phase angle plots of the Al–Si and Zn coated steels after immersion in 3.5 wt% NaCl solution. The Bode response provides detailed information regarding electrochemical stability, coating integrity, and interfacial corrosion behavior of the coating systems during immersion.

For both Al–Si coated steels (Fig. 6a and b), relatively high impedance modulus values were maintained in the low-frequency region, indicating effective suppression of charge transfer reactions and superior barrier-type corrosion protection. In particular, the oiled Al–Si specimen exhibited the highest low-frequency impedance magnitude throughout the immersion period, confirming that functional oil treatment significantly enhanced the protective performance of the coating layer. The dense oxide/intermetallic structure formed under the oiled condition likely reduced ionic transport pathways and delayed electrolyte penetration into the coating/substrate interface.

The phase angle plots of the Al–Si specimens showed broad capacitive behavior over a wide frequency range, which is characteristic of stable passive or barrier-type coatings. The wider and more stable phase angle peak observed in the oiled Al–Si specimen suggests improved electrochemical homogeneity and a more ideal capacitive response. Such behavior is generally associated with a dense and uniform surface layer with reduced localized corrosion activity. In contrast, the non-oiled Al–Si specimen exhibited a gradual decrease in phase angle and slight broadening of the response with immersion time, implying progressive interfacial degradation and increasing surface heterogeneity caused by chloride penetration through coating defects or microcracks.

The Zn coated steel (Fig. 6c) exhibited substantially lower impedance modulus values compared with the Al–Si coated specimens, particularly in the low-frequency region. This result indicates lower overall corrosion resistance and faster electrochemical degradation during immersion. In addition, the phase angle peak of the Zn specimen was narrower and shifted toward higher frequency regions, suggesting less stable capacitive behavior and the development of localized electrochemical reactions associated with Zn dissolution.

The appearance of depressed phase angle behavior and reduced impedance in the Zn coating can be attributed to the sacrificial corrosion mechanism of Zn-containing phases. Initially, the Zn-rich coating provides cathodic protection through preferential anodic dissolution; however, progressive Zn consumption during immersion leads to coating discontinuity and localized electrochemical heterogeneity. As a result, the interfacial corrosion process becomes increasingly dominated by active dissolution rather than stable barrier protection.

Overall, the Bode plot analysis clearly demonstrates that the Al–Si coatings exhibit corrosion protection behavior dominated by stable oxide/intermetallic barrier layers, whereas the Zn coating undergoes active sacrificial dissolution in chloride-containing environments. Furthermore,

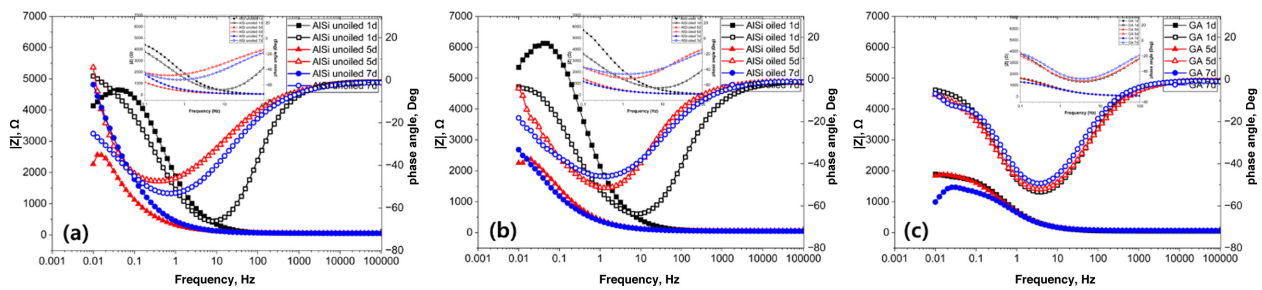

Fig. 6. Bode plots of (a) non-oiled Al–Si coated steel, (b) oiled Al–Si coated steel, and (c) Zn coated steel measured after immersion in 3.5 wt% NaCl solution for 1, 5, and 7 days

the functional oil treatment effectively improved the electrochemical stability of the Al–Si coating by promoting the formation of a more homogeneous and protective surface layer during hot press forming.

The equivalent electrical circuit (EEC) shown in Fig. 7 was employed to analyze the electrochemical impedance behavior of the coated hot stamping steels in 3.5 wt% NaCl solution. The circuit consists of the solution resistance (R_s) connected in series with a parallel combination of the constant phase element (CPE_1) and resistance component (R_1), representing the electrochemical response of the coating/electrolyte interface. Although coated systems generally exhibit separate impedance responses associated with the coating layer and substrate interface, only a single depressed capacitive loop was observed in the present Nyquist plots. This suggests that the coating and substrate responses overlapped within the investigated frequency range, making reliable separation difficult. Therefore, a simplified equivalent circuit was employed to represent the dominant corrosion process.

The Rs component corresponds to the electrolyte resistance between the working and reference electrodes and is primarily governed by the conductivity of the NaCl solution. Since the electrolyte composition remained unchanged throughout the experiment, only minor variations in R_s were expected during immersion.

The parallel CPE_1–R_1 element describes the non-ideal capacitive behavior and corrosion resistance of the coating system. The use of the CPE_1 instead of an ideal capacitor account for surface heterogeneity, roughness, localized defects, and non-uniform current distribution at the coating interface. The CPE exponent (n) provides information regarding the deviation from ideal capacitive behavior, where values approaching unity indicate a more homogeneous and electrochemically stable surface condition.

The R_1 component represents the overall resistance associated with the coating barrier and interfacial charge transfer process. Therefore, higher R_1 values indicate improved corrosion resistance and stronger suppression of electrochemical reactions at the coating/substrate interface. In the present study, the oiled Al–Si coated specimen exhibited the highest R_1 values, indicating that functional oil treatment enhanced the integrity and barrier performance of the oxide/intermetallic layer formed during hot press forming.

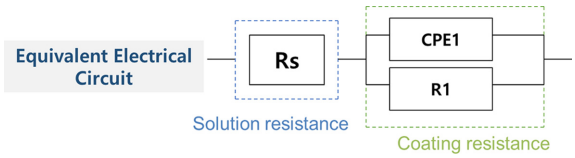

Fig. 7. Equivalent electrical circuit (EEC) used for fitting the electrochemical impedance spectroscopy (EIS) data, consisting of solution resistance (R_s), constant phase element (CPE_1), and coating/charge transfer resistance (R_1)

From an electrochemical perspective, the simplified single time-constant circuit suggests that the corrosion behavior of the Al–Si coated steels was predominantly governed by barrier-type protection through oxide/intermetallic layers. In contrast, the lower resistance and more unstable impedance behavior observed in the Zn coated steel indicate accelerated interfacial degradation associated with sacrificial Zn dissolution and localized corrosion activity.

Table 1 summarizes the fitted EIS parameters obtained from the equivalent circuit analysis for the coated hot stamping steels immersed in 3.5 wt% NaCl solution. The values shown in parentheses represent the fitting error (%) obtained from the equivalent circuit fitting and were included to evaluate the reliability of the fitted parameters. The fitting errors for all parameters were generally maintained below ~5%, indicating good agreement between the experimental spectrum and the proposed equivalent electrical circuit model.

The solution resistance (R_s) remained relatively stable regardless of immersion time or coating condition, ranging from approximately 39–47 $\Omega \cdot cm^2$ for all specimens This behavior can be attributed that the electrolyte conductivity remained nearly constant throughout the immersion test, and therefore the corrosion behavior was mainly governed by interfacial electrochemical reactions rather than changes in solution resistance.

For the Al–Si coated steels, the oiled specimen exhibited the highest interfacial resistance (R_1) at the initial immersion stage, reaching approximately 6334 $\Omega \cdot cm^2$ after 1 day of immersion. Although the R_1 value decreased to 2774 $\Omega \cdot cm^2$ after 5 days, it remained relatively high at 3517 $\Omega \cdot cm^2$ after 7 days, demonstrating sustained barrier-type corrosion protection. In comparison, the non-oiled Al–Si specimen exhibited R_1 values of 4637, 3544,

Table 1. Fitted electrochemical impedance spectroscopy (EIS) parameters obtained from equivalent electrical circuit analysis for non-oiled Al–Si, oiled Al–Si, and Zn coated steels after immersion in 3.5 wt% NaCl solution for 1, 5, and 7 days

Sample	Immersion time	R_s ($\Omega \cdot cm^2$)	CPE_1-Q ($\Omega^{-1} \cdot s^n \cdot cm^{-2}$)	CPE_1-n	R_1 ($\Omega \cdot cm^2$)
AlSi unoiled	1d	46.00 (0.46)	9.150e-04 (1.05)	0.852 (0.28)	4637 (0.65)
	5d	46.21 (1.25)	9.816e-04 (2.18)	0.646 (1.12)	3544 (5.16)
	7d	41.77 (0.44)	6.777e-04 (0.65)	0.666 (0.32)	6915 (1.83)
AlSi oiled	1d	47.19 (0.50)	8.924e-04 (1.03)	0.807 (0.29)	6334 (0.74)
	5d	46.06 (0.43)	6.707e-04 (0.83)	0.708 (0.37)	2774 (1.14)
	7d	39.42 (0.22)	8.828e-04 (0.37)	0.620 (0.18)	3517 (0.78)
Zn coated	1d	44.75 (0.13)	2.966e-04 (0.33)	0.766 (0.11)	1896 (0.22)
	5d	42.83 (0.25)	3.360e-04 (0.59)	0.737 (0.20)	1955 (0.43)
	7d	42.83 (0.25)	3.258e-04 (2.26)	0.759 (0.78)	1418 (1.36)

and 6915 $\Omega \cdot cm^2$ after 1, 5, and 7 days, respectively. The increase in R_1 after 7 days immersion may be associated with the formation of secondary corrosion products or thickened oxide layers that partially suppressed charge transfer reactions at the interface.

The CPE_1-Q values for the Al–Si coated steels increased with immersion time. For example, the oiled Al–Si specimen exhibited CPE_1-Q values increasing from 8.944×10^{-5} to 8.828×10^{-4} $\Omega^{-1} \cdot s^n \cdot cm^{-2}$ between 1 and 7 days. Similarly, the non-oiled Al–Si specimen showed an increase from 9.150×10^{-5} to 6.777×10^{-4} $\Omega^{-1} \cdot s^n \cdot cm^{-2}$. This increase indicates progressive electrolyte penetration and increases interfacial capacitance due to gradual degradation of the oxide/intermetallic layer.

The CPE_1-n values of the Al–Si specimens gradually decreased with immersion time, from 0.807 to 0.620 for the oiled specimen and from 0.852 to 0.666 for the non-oiled specimen. The decrease in n suggests increasing surface heterogeneity and deviation from ideal capacitive behavior caused by localized chloride attack and interfacial degradation. Nevertheless, the relatively high R_1 values indicate that the Al-rich oxide/intermetallic layers still maintained effective barrier protection during immersion.

In contrast, the Zn coated steel exhibited significantly lower R_1 values compared with the Al–Si coatings, decreasing from 1896 $\Omega \cdot cm^2$ after 1 day to 1418 $\Omega \cdot cm^2$ after 7 days. The relatively low resistance indicates inferior barrier performance due to active Zn dissolution in the chloride-containing environment. The Zn specimen also showed comparatively high CPE_1-Q values (~3×10^{-4} $\Omega^{-1} \cdot s^n \cdot cm^{-2}$) and lower capacitive stability, suggesting continuous electrochemical activity associated with sacrificial corrosion behavior and localized degradation.

Overall, the fitted EIS parameters quantitatively confirm that the Al–Si coated steels exhibited superior corrosion resistance compared with the Zn coating. Furthermore, functional oil treatment improved the electrochemical stability of the Al–Si coating by enhancing the integrity of the oxide/intermetallic layer formed during hot press forming.

Fig. 8. presents the potentiodynamic polarization behavior of the Al–Si and Zn coated steels after immersion in 3.5 wt% NaCl solution. The polarization response clearly reveals the distinct electrochemical corrosion mechanisms associated with the barrier-type Al–Si coating and the sacrificial Zn-based coating.

Both Al–Si coated steels exhibited relatively noble

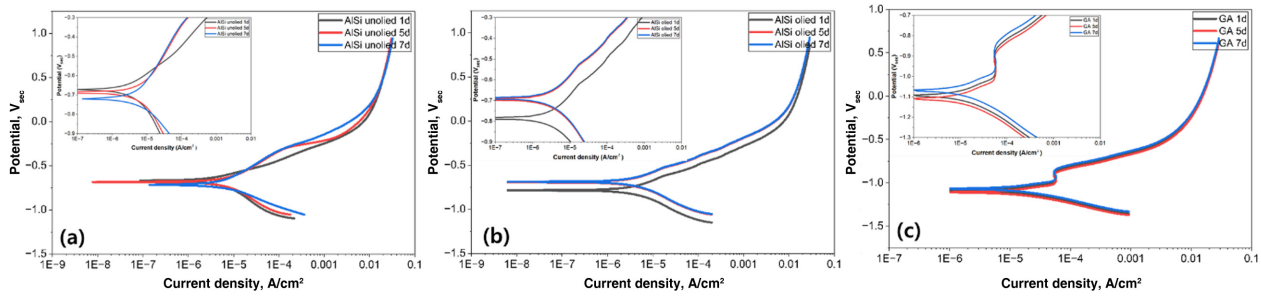

Fig. 8. Potentiodynamic polarization curves of (a) non-oiled Al–Si coated steel, (b) oiled Al–Si coated steel, and (c) Zn coated steel after immersion in 3.5 wt% NaCl solution for 1, 5, and 7 days
***footnote : Values in parentheses indicate the fitting error (%) associated with each parameter obtained from equivalent circuit fitting**

corrosion potentials (E_{corr}) and lower corrosion current densities (I_{corr}) compared with the Zn coated steel, indicating superior corrosion resistance and lower electrochemical dissolution kinetics. In particular, the oiled Al–Si specimen (Fig. 8b) maintained the lowest anodic current density and the broadest passive-like behavior throughout immersion, demonstrating enhanced electrochemical stability resulting from functional oil treatment. The anodic branches of the Al–Si coated specimens showed gradual current increases without abrupt active dissolution behavior. This characteristic response is attributed to the formation of stable Al-rich oxide layers and Fe–Al intermetallic compounds during hot press forming. These layers act as an effective physical barrier against chloride ion penetration and suppress direct electrochemical reactions at the coating/substrate interface.

For the non-oiled Al–Si specimen (Fig. 8a), the anodic current density increased progressively with immersion time, indicating gradual deterioration of the protective oxide/intermetallic layer. Chloride penetration through microcracks and localized coating defects likely accelerated interfacial degradation during prolonged immersion. Nevertheless, the specimen still maintained relatively low current densities compared with the Zn coating, confirming the intrinsic barrier capability of the Al–Si coating system. The oiled Al–Si specimen exhibited comparatively lower anodic current densities over the entire immersion period, suggesting that functional oil treatment promoted the formation of a denser and more homogeneous oxide layer during HPF processing. Such a compact surface layer effectively reduced active dissolution kinetics and suppressed localized corrosion propagation. This result is consistent with the higher impedance magnitude and larger charge transfer resistance observed in the EIS analysis.

In contrast, the Zn coated steel (Fig. 8c) exhibited significantly more active polarization behavior characterized by higher anodic current densities and more negative corrosion potentials. This behavior is typical of sacrificial Zn dissolution in chloride-containing environments. Initially, Zn preferentially dissolves to cathodically protect the steel substrate; however, progressive Zn consumption during immersion promotes coating discontinuity and localized electrochemical heterogeneity.

Furthermore, the Zn specimen showed unstable anodic behavior without a distinct passive region, indicating that the corrosion process was dominated by continuous active dissolution rather than stable passive film formation. The relatively high current density observed during anodic polarization suggests accelerated degradation of the Zn-containing surface layer and reduced long-term corrosion protection capability.

Overall, the polarization results demonstrate that the Al–Si coatings provide corrosion protection primarily through stable barrier-type oxide/intermetallic layers, whereas the Zn coating relies on sacrificial anodic dissolution of Zn. Moreover, functional oil treatment significantly enhanced the corrosion resistance of the Al–Si coated steel by stabilizing the surface oxide structure and suppressing electrochemical dissolution during immersion.

The Tafel extrapolation of the polarization curves provides quantitative support for the above interpretation in Table 2. From the exact fitting values, the polarization curves clearly indicate that the Al–Si-coated specimen

Table 2. Electrochemical parameters obtained from potentiodynamic polarization analysis for non-oiled Al–Si, oiled Al–Si, and Zn coated steels after immersion in 3.5 wt% NaCl solution for 1, 5, and 7 days

Sample	Condition	E_{corr} (V_{SCE})	i_{corr} (A/cm^2)	β_a (mV/dec)	β_c (mV/dec)
AlSi unoiled	1d	-0.656	2.425e-06	118.58	214.10
	5d	-0.675	3.655e-06	168.10	227.42
	7d	-0.691	3.179e-06	163.30	177.08
AlSi oiled	1d	-0.771	2.053e-06	150.58	191.20
	5d	-0.675	5.116e-06	185.49	200.53
	7d	-0.637	5.856e-06	152.08	232.90
Zn coated	1d	-1.087	9.949e-06	173.29	136.64
	5d	-1.063	1.620e-05	257.84	125.08
	7d	-1.132	1.121e-05	215.82	138.87

has a lower corrosion current density (i_{corr}) and a more noble corrosion potential (E_{corr}) than the Zn-coated specimen. A lower I_{corr} value for the Al–Si-coated specimen implies a lower corrosion rate, confirming its superior corrosion resistance. In contrast, the higher I_{corr} of the Zn-coated specimen reflects accelerated corrosion kinetics associated with sacrificial Zn dissolution.

Table 2 summarizes the electrochemical parameters obtained from Tafel extrapolation of the potentiodynamic polarization curves, including E_{corr}, I_{corr}, and anodic/cathodic Tafel slopes (β_a and β_c). The extracted parameters quantitatively demonstrate the differences in corrosion behavior between the Al–Si and Zn coated steels under chloride-containing environments.

The Zn coated steel exhibited the most negative E_{corr} values throughout immersion, ranging from −1.087 to −1.132 V_{SCE}, confirming the highly active electrochemical behavior of the Zn-based coating. Such negative corrosion potentials are characteristic of sacrificial anodic dissolution, where Zn preferentially corrodes to cathodically protect the steel substrate. In contrast, the Al–Si coated steels showed significantly more noble E_{corr} values between approximately −0.63 and −0.77 V_{SCE}, indicating improved thermodynamic stability due to the presence of stable Al-rich oxide and Fe–Al intermetallic layers.

The I_{corr}, which reflects the overall corrosion kinetics, was substantially higher for the Zn coating than for the Al–Si coated specimens. The Zn specimen exhibited I_{corr} values of 9.949×10^{-6}, 1.620×10^{-5}, and 1.121×10^{-5} A/cm^2 after 1, 5, and 7 days of immersion, respectively. These values are approximately one order of magnitude higher than those of the Al–Si coated steels, indicating accelerated anodic dissolution and reduced corrosion resistance in the chloride environment.

Among the Al–Si coated specimens, the non-oiled condition exhibited relatively stable corrosion current densities ranging from 2.425×10^{-6} to 3.655×10^{-6} A/cm^2 during immersion. Meanwhile, the oiled Al–Si specimen showed an initially lower I_{corr} value of 2.053×10^{-6} A/cm^2 after 1 day, suggesting improved initial barrier performance due to functional oil treatment. However, the I_{corr} values increased to 5.116×10^{-6} and 5.856×10^{-6} A/cm^2 after 5 and 7 days, respectively, implying gradual degradation of the oxide/intermetallic layer during prolonged chloride exposure.

The anodic Tafel slope (β_a) values generally increased with immersion time, particularly for the Zn specimen, which exhibited βa values up to 257.84 mV/dec after 5 days. This behavior suggests increasing anodic polarization resistance associated with corrosion product accumulation and localized Zn dissolution during immersion. In contrast, the Al–Si coated specimens showed relatively moderate βa values, indicating more stable anodic behavior governed by passive or barrier-type surface layers.

The cathodic Tafel slopes (β_c) of the Al–Si coated steels were generally higher than those of the Zn coating, suggesting suppressed cathodic oxygen reduction kinetics due to the dense oxide/intermetallic surface layers. Particularly, the oiled Al–Si specimen exhibited βc values exceeding 230 mV/dec after 7 days immersion, indicating enhanced resistance against cathodic electrochemical

reactions.

Overall, the polarization parameters quantitatively confirm that the Al–Si coated steels exhibited superior corrosion resistance compared with the Zn coating in 3.5 wt% NaCl solution. The corrosion behavior of the Al–Si coatings was primarily governed by barrier-type oxide/intermetallic protection, whereas the Zn coating exhibited active sacrificial dissolution behavior dominated by Zn corrosion. Furthermore, functional oil treatment improved the initial electrochemical stability of the Al–Si coating by reducing corrosion current density and promoting formation of a more protective surface layer after hot press forming.

3.3 Surface analysis and corrosion mechanisms

Fig. 9 presents the post-corrosion surface morphologies of the Al–Si and Zn coated steels after 7 days of immersion in 3.5 wt% NaCl solution. Distinct differences in corrosion morphology and corrosion product formation were observed depending on coating type and oil treatment condition, indicating fundamentally different corrosion degradation mechanisms.

The non-oiled Al–Si specimen (Fig. 9 a_1–a_3) exhibited severe localized degradation characterized by large cavities, porous corrosion products, and locally collapsed surface regions. At higher magnification, irregular pit-like features and loosely packed corrosion products were observed around the damaged regions. These morphologies suggest that chloride ions penetrated through defects and microcracks within the Fe–Al intermetallic/oxide layer, resulting in localized interfacial corrosion beneath the coating. The porous corrosion products formed inside the cavities indicate unstable corrosion product accumulation and repeated electrolyte ingress during immersion. Such localized attack is consistent with the gradual decrease in impedance and

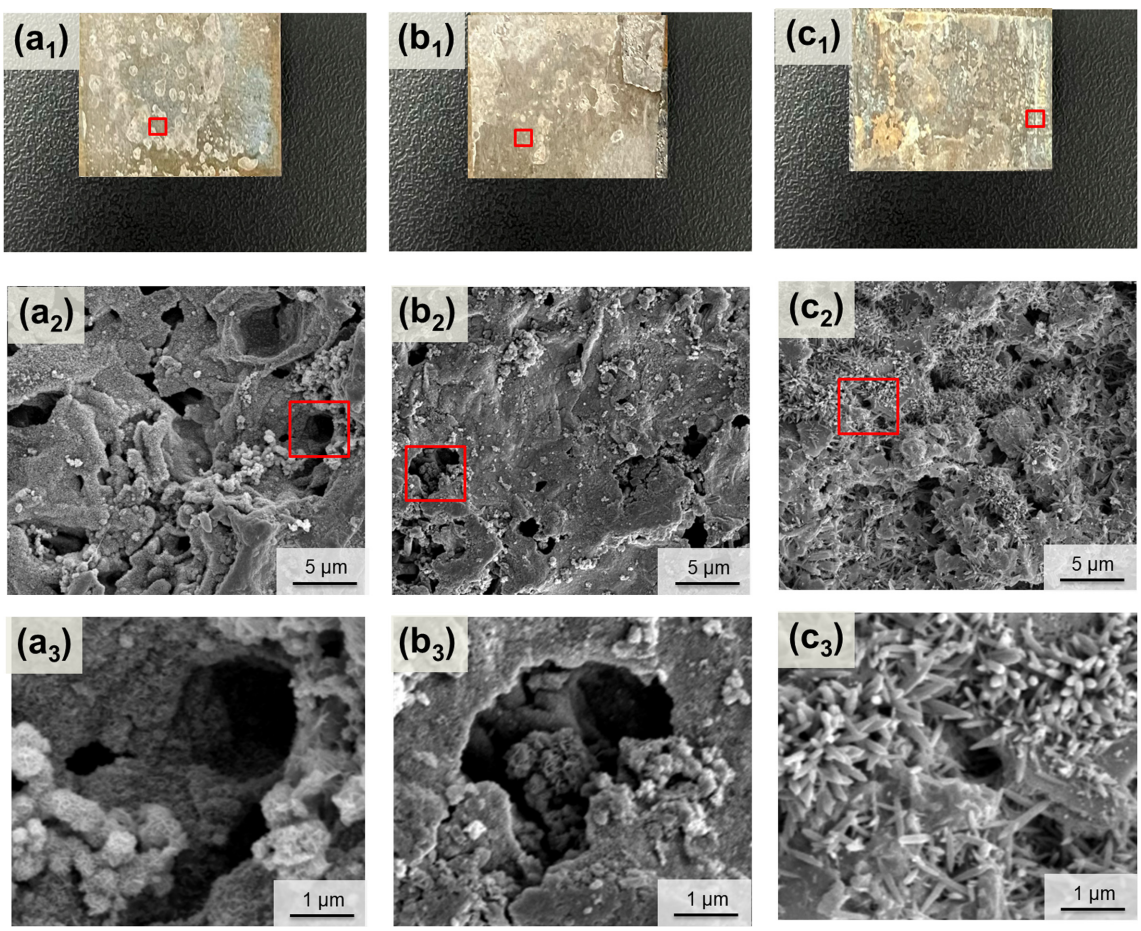

Fig. 9. Surface morphologies of coated hot stamping steels after 7 days of immersion in 3.5 wt% NaCl solution: (a_1–a_3) non-oiled Al–Si coated steel, (b_1–b_3) oiled Al–Si coated steel, and (c_1–c_3) Zn coated steel at different magnifications

increasing electrochemical heterogeneity observed in the EIS analysis.

The oiled Al–Si specimen (Fig. 9 b_1–b_3) also exhibited localized corrosion features; however, the damaged regions appeared comparatively smaller and more compact than those of the non-oiled specimen. The corrosion products were denser and less porous, suggesting improved stability of the oxide/intermetallic layer formed under the functional oil condition. The refined corrosion morphology implies that functional oil treatment suppressed direct chloride penetration and delayed localized corrosion propagation during immersion. This result is in good agreement with the higher impedance magnitude and larger charge transfer resistance observed for the oiled Al–Si specimen in the electrochemical measurements.

In contrast, the Zn coated steel (Fig. 9 c_1–c_3) exhibited a markedly different corrosion morphology dominated by widespread surface degradation and the formation of needle-like corrosion products. The acicular corrosion products are characteristic of Zn-based corrosion compounds such as simonkolleite or Zn hydroxide chloride species formed during sacrificial Zn dissolution in chloride-containing environments. Unlike the localized cavities observed in the Al–Si coatings, the Zn specimen showed more uniformly distributed but electrochemically active surface degradation. This behavior indicates continuous Zn dissolution and corrosion product precipitation over the entire surface during immersion.

The morphological differences observed strongly support the electrochemical results. The Al–Si coatings primarily underwent localized corrosion associated with barrier layer breakdown at defective regions, whereas the Zn coating experienced active sacrificial dissolution accompanied by extensive Zn corrosion product formation. Furthermore, the improved surface integrity observed in the oiled Al–Si specimen demonstrates that functional oil treatment enhanced the durability of the oxide/intermetallic layer and effectively suppressed chloride-induced localized corrosion after hot press forming.

The corrosion behavior observed in the present study is closely associated with the distinct protection mechanisms of Al–Si and Zn-based coatings reported in previous studies. Windmann *et al.* [16] reported that Al–Si coated hot stamping steels form Fe–Al intermetallic compounds such as Al_5Fe_2 and AlFe during austenitization, which contribute to oxidation resistance through the development of stable Al-rich oxide layers. Similarly, the present study confirmed that the Al–Si coated steels exhibited relatively noble corrosion potentials, higher impedance values, and lower corrosion current densities compared with the Zn coated steel, indicating dominant barrier-type corrosion protection.

Previous studies have also demonstrated that the corrosion resistance of Al–Si coatings strongly depend on the integrity and compactness of the oxide/intermetallic layer formed after hot press forming. C. Ju *et al.* [17] reported that localized corrosion in Al–Si coated press hardened steels preferentially initiates at coating defects or intermetallic cracking regions where chloride ions can penetrate the coating/substrate interface. This mechanism is consistent with the localized pit-like corrosion morphologies observed in the present study, particularly for the non-oiled Al–Si specimen after 7 days immersion.

The improved electrochemical stability observed in the oiled Al–Si specimen can be attributed to the formation of a thicker and more homogeneous oxide layer during HPF processing. Similar behavior has been reported by M. N. Sanath *et al.* [18], who suggested that surface condition and oxide morphology critically influence electrolyte penetration and long-term coating stability in Al–Si coated hot stamping steels. The higher impedance magnitude and larger charge transfer resistance observed in the oiled specimen in the present work support this interpretation.

In contrast, the Zn coated steel exhibited electrochemical behavior characteristic of sacrificial Zn dissolution. Thierry *et al.* [19] reported that Zn-coated steels in chloride-containing environments undergo preferential anodic dissolution accompanied by the formation of Zn hydroxide chloride corrosion products such as simonkolleite. In the present study, the Zn specimen exhibited significantly more negative corrosion potentials, lower impedance values, and acicular corrosion products after immersion, indicating active Zn corrosion and progressive coating degradation.

Furthermore, LeBozec *et al.* [20] suggested that heterogeneous Zn dissolution and corrosion product accumulation can accelerate localized electrochemical

instability in galvanized steels exposed to chloride environments. This mechanism explains the unstable anodic behavior and relatively low interfacial resistance observed for the Zn coating in the present study. Therefore, the overall results indicate that the corrosion resistance of coated hot stamping steels is strongly governed by the stability of the oxide/intermetallic layer and the dominant corrosion protection mechanism, namely barrier-type protection for Al–Si coatings and sacrificial protection for Zn-based coatings.

Fig. 10 schematically summarizes the corrosion protection mechanisms and degradation behavior of Al–Si and Zn coated hot stamping steels after hot press forming (HPF) in chloride-containing environments. The overall corrosion behavior was strongly influenced by coating chemistry, interfacial layer evolution during HPF, and functional oil treatment.

For the Al–Si coated steels, high-temperature austenitization during HPF promoted the formation of Fe–Al intermetallic compounds (primarily Al_5Fe_2 and AlFe) together with an outer Al-rich oxide layer. These multilayered structures acted as an effective physical barrier against chloride penetration and suppressed direct electrochemical reactions at the steel substrate. In particular, the oiled Al–Si specimen developed a thicker Al-oxide layer compared with the non-oiled condition, indicating that functional oil treatment significantly influenced oxidation behavior during thermal processing. The electrochemical analyses consistently demonstrated that the Al–Si coatings exhibited superior corrosion resistance compared with the Zn coating. The oiled Al–Si specimen showed the most noble OCP, the highest impedance magnitude, the largest Nyquist semicircle diameter, and the highest interfacial resistance, indicating enhanced barrier performance and improved electrochemical stability. The dense oxide/intermetallic layer formed under the oiled condition effectively reduced electrolyte penetration and delayed charge transfer reactions during immersion. However,

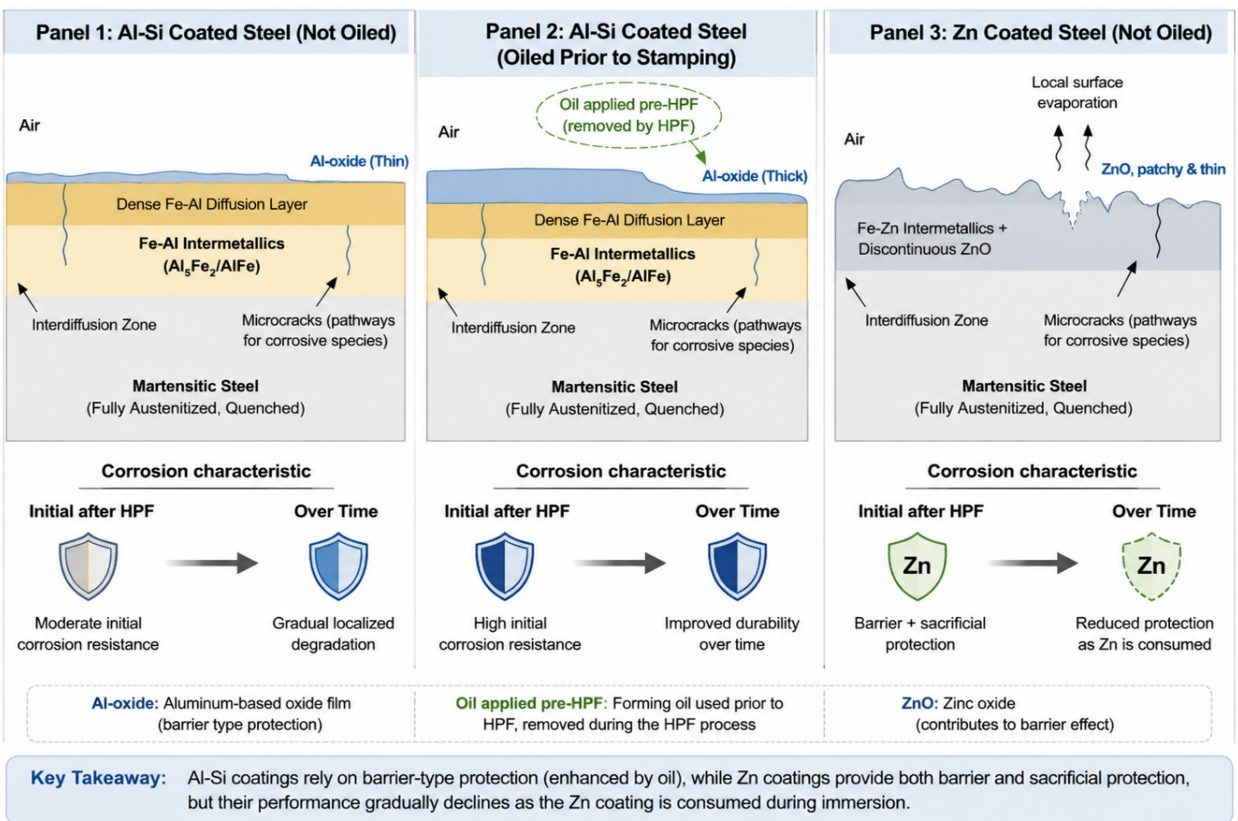

Fig. 10. Schematic illustration of the corrosion mechanisms of Al–Si and Zn coated hot stamping steels after HPF in 3.5 wt% NaCl solution. Al–Si coatings exhibit barrier-type protection through Al-rich oxide and Fe–Al intermetallic layers, whereas Zn coatings show sacrificial corrosion behavior through Zn dissolution. Functional oil treatment promoted formation of a thicker oxide layer and improved corrosion resistance

despite the improved initial corrosion resistance, localized degradation was still observed in the Al–Si coatings after 7days immersion. Surface SEM observations revealed pit-like cavities and porous corrosion products associated with chloride ingress through coating defects and microcracks within the brittle Fe–Al intermetallic layer. Therefore, the corrosion mechanism of the Al–Si coating can be described as a barrier-dominated protection system controlled by localized breakdown of the oxide/intermetallic layer.

Although the oiled Al–Si specimen exhibited improved electrochemical performance and a relatively thicker oxide layer, the present study does not directly verify differences in oxide chemistry or elemental distribution. Previous studies have reported that the corrosion resistance of Al–Si coatings is strongly influenced by the composition, continuity, and stability of surface oxide layers, which are commonly characterized using surface analytical techniques such as XPS and AES [21]. Therefore, the enhanced corrosion resistance observed in the oiled specimen is interpreted as being associated with improved barrier characteristics of the oxide layer. Further investigation using surface chemical analyses would be beneficial to clarify the detailed role of functional oil treatment on oxide formation and corrosion protection mechanisms.

In contrast, the Zn coated steel exhibited a fundamentally different corrosion mechanism governed by sacrificial Zn dissolution. During HPF, Zn evaporation and Fe–Zn interdiffusion generated heterogeneous interfacial structures with discontinuous ZnO regions and localized defects. As a result, the Zn coating showed significantly more negative corrosion potentials and lower impedance values than the Al–Si coatings throughout immersion.

The electrochemical behavior of the Zn coating was characterized by active anodic dissolution rather than stable passive behavior. Although the Zn-rich coating initially provided cathodic protection to the steel substrate, progressive Zn dissolution during immersion gradually depleted the sacrificial coating layer and reduced its long-term protective capability. SEM observations further confirmed the formation of acicular Zn-based corrosion products, likely simonkolleite or Zn hydroxide chloride compounds, indicating continuous sacrificial corrosion and subsequent corrosion product accumulation on the surface. Therefore, the corrosion performance of the Zn coating was controlled primarily by sacrificial anodic protection, whereas the Al–Si coating exhibited corrosion resistance through a barrier-type protection mechanism.

Overall, the present results clearly demonstrate that the corrosion resistance of hot stamping steels is governed not only by coating composition but also by post-HPF surface evolution and interfacial stability. The Al–Si coatings primarily provide barrier-type protection through stable oxide/intermetallic layers, whereas the Zn coating relies on sacrificial anodic dissolution of Zn. Furthermore, functional oil treatment significantly improved the electrochemical stability of the Al–Si coating by promoting formation of a thicker and more homogeneous oxide layer during HPF processing, thereby delaying chloride-induced localized corrosion propagation.

4. Conclusions

The corrosion behavior and surface/interfacial microstructural evolution of hot press formed (HPF) steels were systematically evaluated through combined electrochemical and microstructural analyses. The main conclusions of this study are summarized as follows:

Al–Si coated steels exhibited significantly higher corrosion resistance than Zn coated steel in 3.5 wt% NaCl solution due to the formation of stable Al-rich oxide and Fe–Al intermetallic layers after hot press forming.

Functional oil treatment promoted the formation of a thicker and more homogeneous Al-oxide layer, resulting in higher impedance, lower corrosion current density, and improved electrochemical stability during immersion.

Electrochemical analyses (OCP, EIS, and potentiodynamic polarization) confirmed that the corrosion protection mechanism of Al–Si coatings was dominated by barrier-type passive protection, whereas Zn coating behavior was governed by sacrificial Zn dissolution.

The Zn coated steel exhibited more negative corrosion potentials, lower charge-transfer resistance, and extensive formation of Zn-based corrosion products, indicating that its corrosion behavior was primarily governed by sacrificial Zn dissolution. Progressive consumption of the Zn-rich coating reduced the overall barrier effectiveness during immersion.

Surface observations after immersion revealed that corrosion in Al–Si coatings mainly occurred through localized breakdown of the oxide/intermetallic layer at defective regions, while functional oil treatment effectively delayed chloride-induced localized corrosion propagation.

These findings suggest that functional oil-assisted Al–Si coatings can be effectively applied to automotive hot stamping components requiring enhanced long-term corrosion durability under chloride-containing service environments. Furthermore, optimization of post-HPF surface oxide stability is expected to be an important strategy for improving durability and reliability of ultra-high-strength steel components.

Acknowledgments

This work was supported by Korea institute for Advancement of Technology (KIAT) grant funded by the Korea Government(MOTIE) (RS-2024-00410332, HRD Program for Industrial Innovation).

References

1. T. Taylor, G. Fourlaris, P. Evans, G. Bright, New generation ultrahigh strength boron steel for automotive hot stamping technologies, *Materials Science and Technology*, **30**, 818 (2014). Doi: https://doi.org/10.1179/1743284713Y.0000000409
2. K. Mori, P. F. Bariani, B.-A. Behrens, A. Brosius, S. Bruschi, T. Maeno, M. Merklein, J. Yanagimoto, Hot stamping of ultra-high strength steel parts, *CIRP Annals*, **66**, 755 (2017). Doi: http://dx.doi.org/10.1016/j.cirp.2017.05.007
3. M. Merklein, J. Lechler, M. Geiger, Characterisation of the flow properties of the quenchable ultra-high-strength steel 22MnB5, *CIRP Annals*, **55**, 229 (2006). Doi: https://10.1016/S0007-8506(07)60404-1
4. H. Karbasian, A. E. Tekkaya, A review on hot stamping, *Journal of Materials Processing Technology*, **210**, 2103 (2010). Doi: https://doi.org/10.1016/j.jmatprotec.2010.07.019
5. P. Hein, J. Wilsius, Status and innovation trends in hot stamping of USIBOR 1500P, *Steel Research International*, **79**, 85 (2008). Doi: https://doi.org/10.1002/srin.200806321
6. ArcelorMittal, Steels for hot stamping — Usibor® and Ductibor® product data, North American Automotive (2026).
7. J. Fan, B. C. De Cooman, State-of-the-knowledge on coating systems for hot stamped parts, *Steel Research International*, **83**, 412 (2012). Doi: https://doi.org/10.1002/srin.201100292
8. C. W. Lee, W. S. Choi, Y. R. Cho, Bruno C. De Cooman, Oxidation behavior and protective coatings for press-hardening steel during austenitization, *Surface and Coatings Technology*, **281**, 35 (2015). Doi: https://doi.org/10.1016/j.surfcoat.2015.09.041
9. W.-J. Cheng, C.-J. Wang, Growth of intermetallic layer in the aluminide-coated/Al–Si-coated hot-stamping steel during austenitization, *Surface and Coatings Technology*, **204**, 824 (2010). Doi: https://doi.org/10.1016/j.surfcoat.2009.09.061
10. S. Wu, Al–Si coating growth in hot-stamping steels: experiments and model, M. A. Sc. thesis, University of Guelph (2021).
11. C. Kim, S. Cho, W. Yang, A. I. Karayan, H. Castaneda, Corrosion behavior of Al-Si-Mg coated hot-press-forming steel, *Corrosion Science*, **183**, 109339 (2021). Doi: https://doi.org/10.1016/j.corsci.2021.109339
12. A. Farooq, U. M. Chaudry, A. Saleem, K. M. Deen, K. Hamad, and R. Ahmad, Sacrificial dissolution of zinc electroplated and cold-galvanized coated steel in saline and soil environments: A Comparison, *Materials*, **14**, 744 (2021). Doi: https://doi.org/10.3390/ma14040744
13. A. Farooq, M. Hamza, Q. Ahmed, K. M. Deen, Evaluating the performance of zinc and aluminum sacrificial anodes in artificial seawater, *Electrochimica Acta*, **314**, 135 (2024). Doi: https://doi.org/10.1016/j.electacta.2019.05.067
14. V. Barranco, S. Feliu Jr., S. Feliu, EIS study of the corrosion behaviour of zinc-based coatings on steel in quiescent 3% NaCl solution. Part 1: directly exposed coating, *Corrosion Science*, **46**, 2203 (2004). Doi: http://10.1016/j.corsci.2003.09.032
15. A. P. Yadav, A. Nishikata, T. Tsuru, Degradation mechanism of galvanized steel in wet–dry cyclic environment containing chloride ions, *Corrosion Science*, **46**, 361 (2004). Doi: https://doi.org/10.1016/S0010-938X(03)00153-7
16. M. Windmann, A. Röttger, W. Theisen, Formation of intermetallic phases in Al-coated hot-stamped 22MnB5 sheets in terms of coating thickness and Si content, *Surface and Coatings Technology*, **24**, 176 (2014). Doi: https://doi.org/10.1016/j.surfcoat.2014.02.056
17. C. Lu, W. Li, H. Wei, H. Gu, Y. Zhang, L. Cui, H. Pan, H. Wang, X. Shen, Y. Liu, Y. Xiao, Time-Dependent Corrosion Behaviors of Al-Si Coated Steel Sheet Under a

Chlorine-Containing Wet–Dry Cycling Environment, *Coatings*, **16**, 631 (2026). Doi: https://doi.org/10.3390/coatings16060631

18. M. N. Sanath, C. L. Nihal, Prabhuling, P. M. Shivaprasad, H. V. Puneeth, M. K. Srinath, Review on Corrosion studies of Heat Treated Al-Si Alloy, *IOP Conference Series: Materials Science and Engineering*, **1258**, 012028 (2022). Doi: http://10.1088/1757-899X/1258/1/012028
19. D. Thierry, D. Persson, C. Leygraf, Atmospheric corrosion of zinc and zinc-alloy coated steels, Encyclopedia of Interfacial Chemistry, pp. 55 - 78, Elsevier, Oxford (2018). Doi: https://doi.org/10.1016/B978-0-12-409547-2.13431-6
20. M. Kouril, P. Pokorny, J. Stoulil, Corrosion Mechanism and Bond-Strength Study on Galvanized Steel in Concrete Environment, *Corrosion Science and Technology*, **16**, 69 (2017). Doi: http://doi.org/10.14773/cst.2017.16.2.69
21. C. Kim, S. Cho, W. Yang, A. I. Karayan, H. Castaneda, Corrosion behavior of Al-Si-Mg coated hot-press-forming steel, *Corrosion Science*, **183**, 109339 (2021). Doi: https://doi.org/10.1016/j.corsci.2021.109339